The Cryosphere

EGU

Supplement of

Retrieval of atmospheric water vapor and temperature profiles over Antarctica from satellite microwave observations using an iterative approach

Zhimeng Zhang et al.

Correspondence to: Zhimeng Zhang (zhimeng@caltech.edu)

Supplement Material

More Comparison With Radiosonde Measurements

5   The Integrated Global Radiosonde Archive comprises radiosonde and pilot balloon observations from multiple stations distributed around the Antarctic coastline. Although the temporal resolution of these radiosonde measurements is lower than that of the ARM campaign, some stations provide data covering the entire year. Davis Station, located at 68.5744°S, 77.9672°E on the east coast, experiences significant variations in surface emissivity (Figure S1). As shown in Figure S3, the ATMS 3db beam at all emission angles (≤60°) partially intersects both the ground and sea ice. During the summer, the melting of sea ice 10   causes a drop in emissivity. Our iterative algorithm can accurately determine the effective surface emissivity for observations over mixed surface types, where traditional retrieval methods lack prior emissivity information. This capability will benefit the atmospheric retrieval.
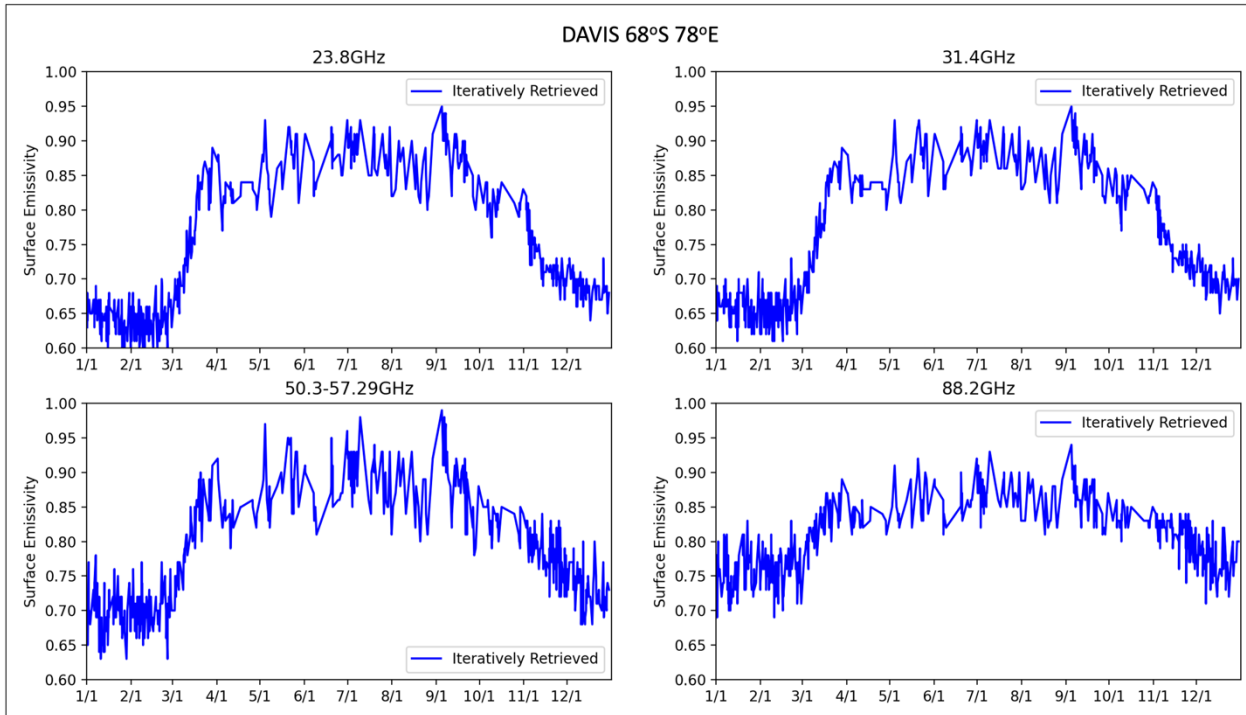
S.1 DAVIS Radiosonde Station

15

Figure S1 Davis Radiosonde Station (68.5744ºS, 77.9672ºE). Surface emissivity from January 2016 to the end of 2016 at three window frequencies (23.8, 31.4 and 88.2 GHz) and the oxygen absorption band (50 – 58GHz). The blue curve represents values from our iterative algorithm. The X-axis shows the month of the year, from 2016/1/1 to 2016/12/31.
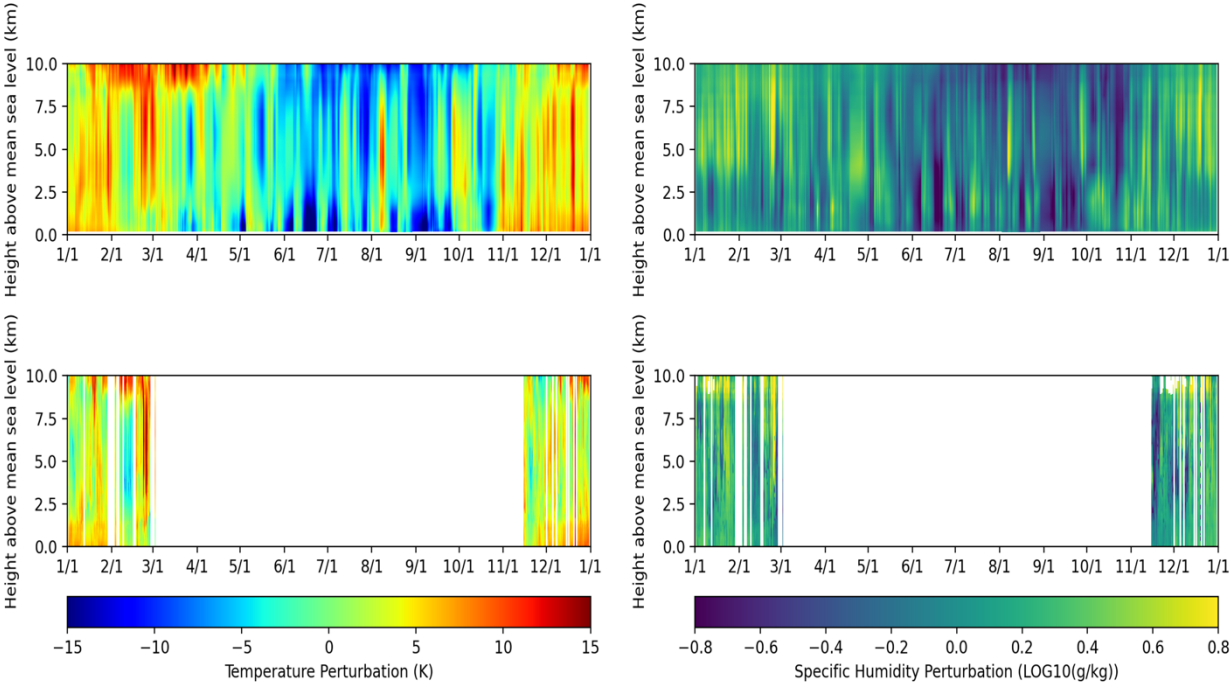
20

Figure S2 Davis Radiosonde Station (68.5744ºS, 77.9672ºE). Temperature and specific humidity perturbations during 2016. The deviations from average values are displayed for that period. The top row presents results from our iterative algorithm, while the bottom row shows data from radiosonde measurements. The X-axis shows the month of the year, from 2016/1/1 to
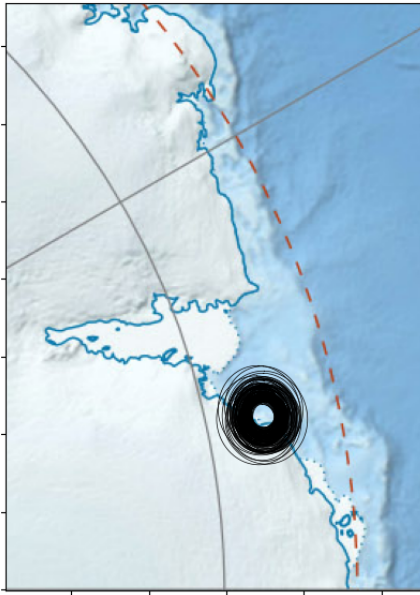25   2016/12/31.

2

Figure S3 ATMS 23.8GHz/31.4GHz 3db footprint at DAVIS radiosonde station at various emission angles ranging from nadir to 60°. The beam width is largest with 5.2° at 23.8GHz/31.4GHz. The beam width is 1.1° for channels in the 160-183 GHz range and 2.2° for the 80GHz and 50-60GHz channels. The elongation of the beam is proportional to $1/_{cos^2\theta}$.
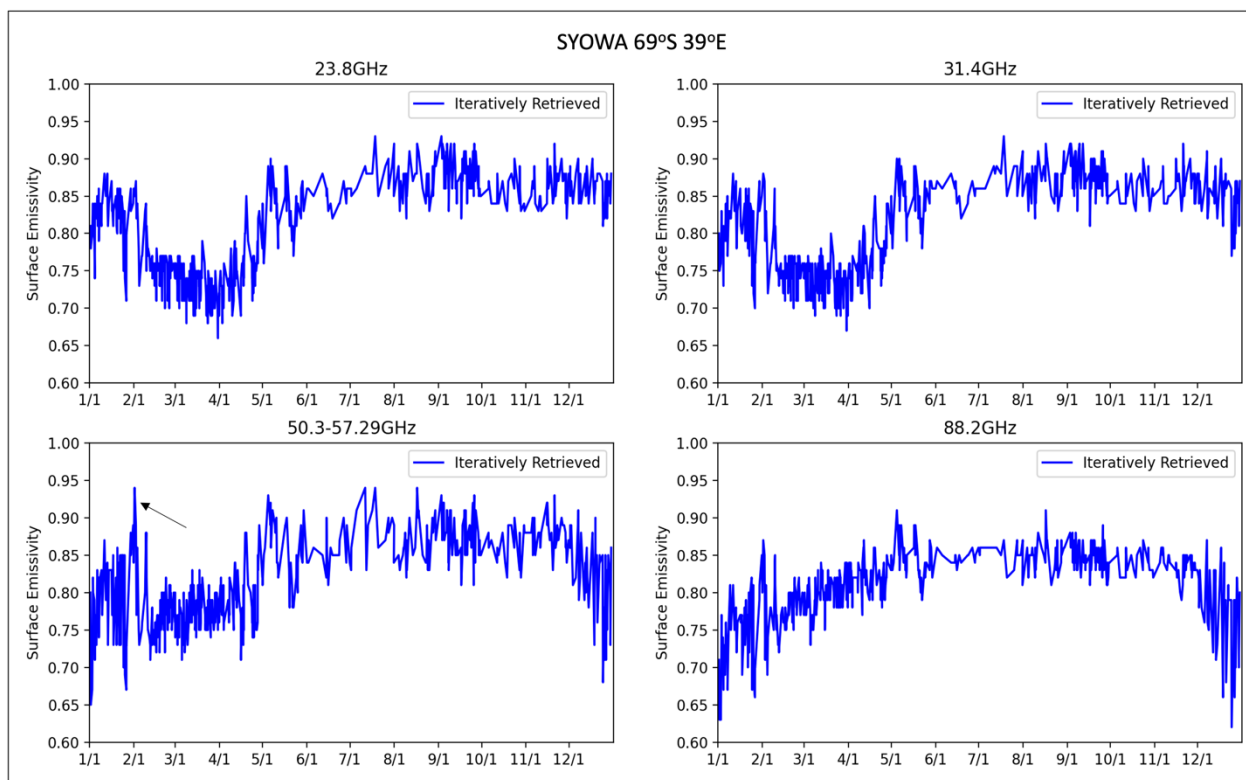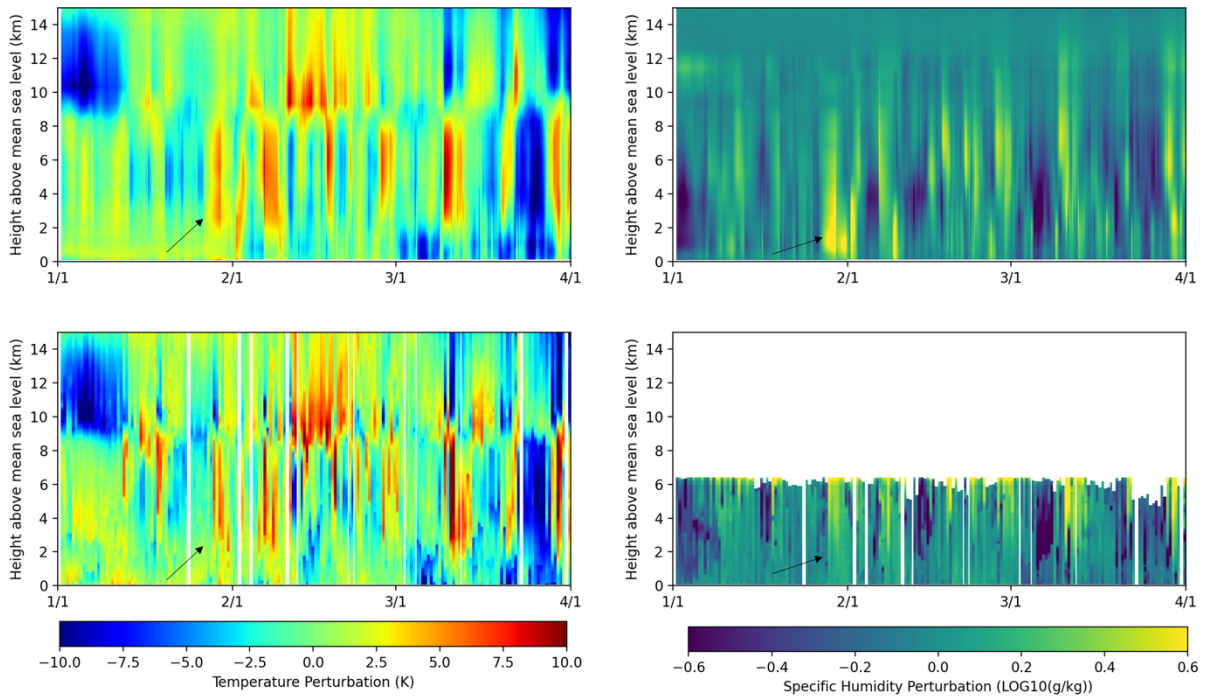
30

S.2 SYOWA Radiosonde Station

Figure S4 Syowa Radiosonde Station (69°S, 39°E). Surface emissivity from January 2016 to the end of 2016 at three window frequencies (23.8, 31.4 and 88.2 GHz) and the oxygen absorption band (50 – 58GHz). The blue curve represents values from our iterative algorithm. The X-axis shows the month of the year, from 2016/1/1 to 2016/12/31. The melting events occurred in mid-January as pointer out by black arrows.

40 **Figure S5** Syowa Radiosonde Station (69ºS, 39ºE). Temperature and specific humidity perturbations during January 2016 to March 2016. The deviations from average values are displayed for that period. The top row presents results from our iterative algorithm, while the bottom row shows data from radiosonde measurements. The X-axis shows the month of the year, from 2016/1/1 to 2016/3/31.
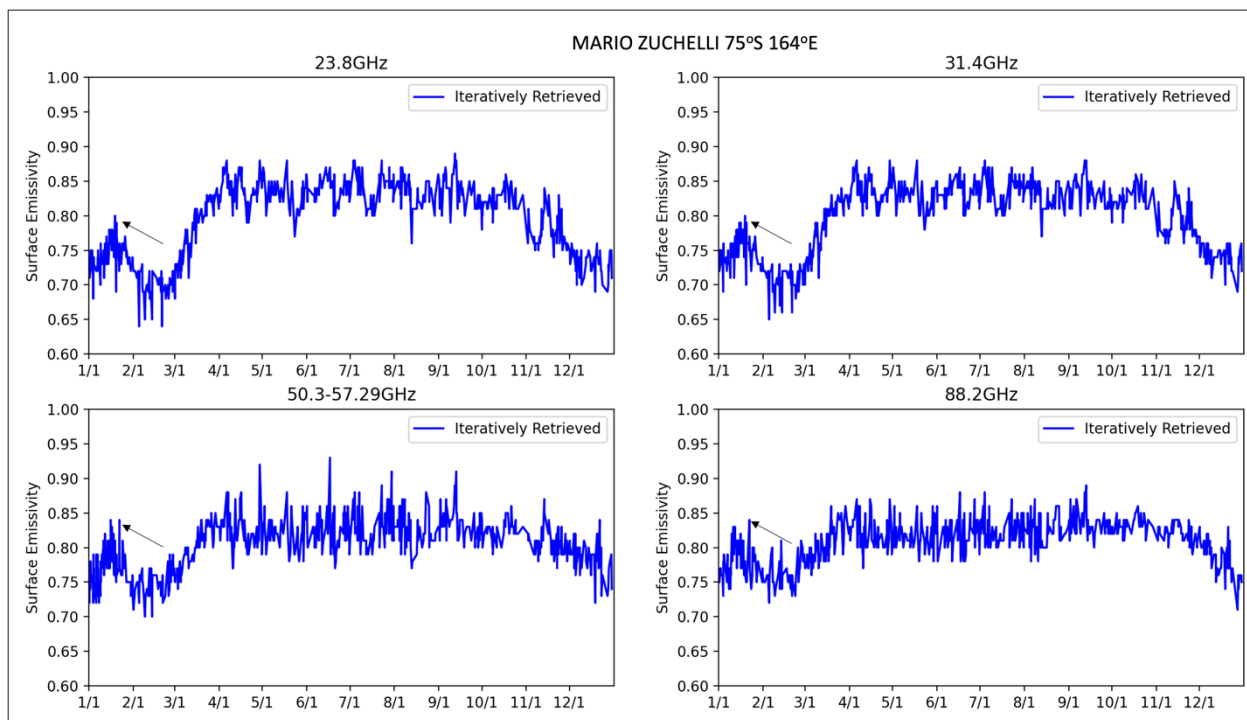
45

S.3 MARIO ZUCHELLI Radiosonde Station

Figure S6 Mario Zuchelli Radiosonde Station (75ºS, 164ºE). Surface emissivity from January 2016 to the end of 2016 at three window frequencies (23.8, 31.4 and 88.2 GHz) and the oxygen absorption band (50 – 58 GHz). The blue curve represents values from our iterative algorithm. The X-axis shows the month of the year, from 2016/1/1 to 2016/12/31. The melting events occurred in mid-January, pointed out by the black arrows.
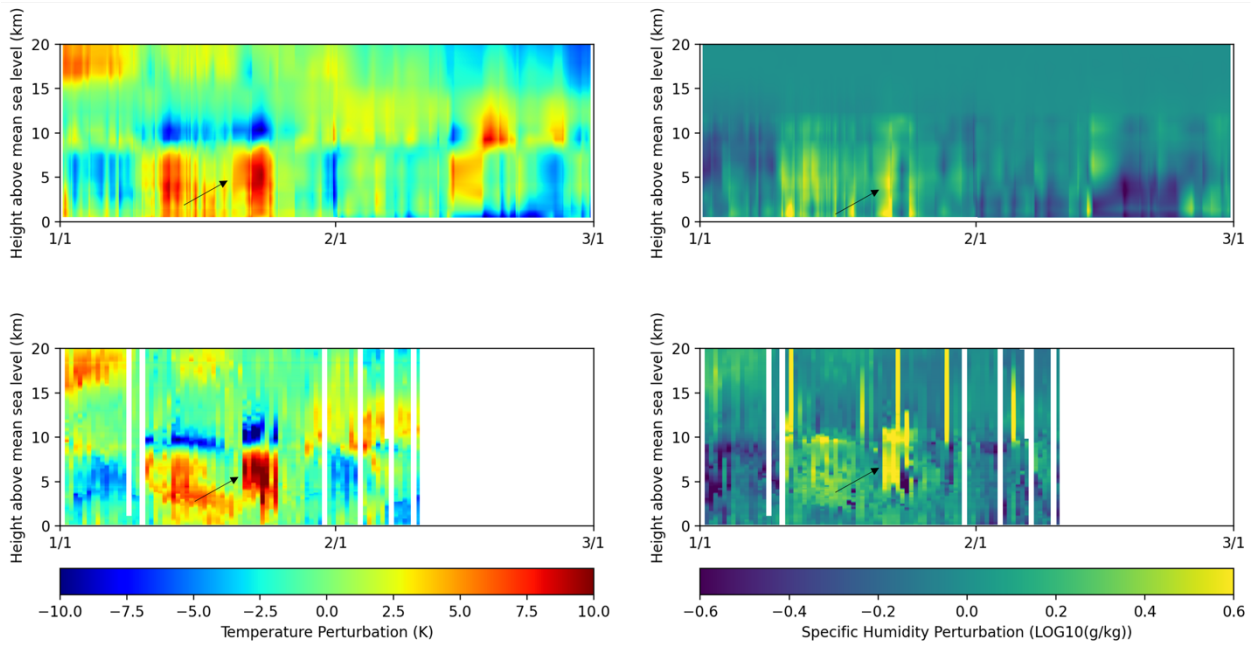
6

Figure S7 Mario Zuchelli Radiosonde Station (75ºS, 164ºE). Temperature and specific humidity perturbations during January and Febuary 2016. The deviations from average values are displayed for that period. The top row presents results from our iterative algorithm, while the bottom row shows data from radiosonde measurements. The X-axis shows the month of the year, from 2016/1/1 to 2016/2/29.